Metabolic models of mixed culture fermentation diagnose bottlenecks and predict strategies for improved medium-chain fatty acid production

Matthew J. Scarborough,[1,2,3] Joshua J. Hamilton,[4] Elizabeth A. Erb,[5] Timothy J. Donohue[1,6] and Daniel R. Noguera[1,2]*

1. The Great Lakes Bioenergy Research Center, UW-Madison, Madison, WI
2. Department of Civil and Environmental Engineering, UW-Madison, Madison, WI
3. Department of Civil and Environmental Engineering, University of Vermont, Burlington, VT
4. Department of Biochemistry, UW-Madison, Madison, WI
5. Department of Chemical and Biological Engineering, UW-Madison, Madison, WI
6. Department of Bacteriology, UW-Madison, Madison, WI

*corresponding author e-mail: mscarbor@uvm.edu

ABSTRACT

Multi-species microbial communities determine the fate of materials in the environment and can be harnessed to produce beneficial products from renewable resources. In a recent example, fermentations by mixed microbial communities have produced medium-chain fatty acids (MCFA). Tools to predict, assess, and improve the performance of these communities, however, are limited. To provide such tools, we constructed two metabolic models of a MCFA-producing community fed a byproduct from a biofuel fermentation. The first model is a unicellular model (iFerment156) that contains a diverse set of fermentation pathways, including reverse β-oxidation for MCFA production while the second model (iFermGuilds564) separates fermentation activities into functional guilds. Both models predicted an energetic advantage for this community to produce octanoic acid as a major fermentation product. Simulations with iFermGuilds564 predicted that 6- and 8-carbon MCFA were largely produced by a sugar-consuming guild, while short-chain fatty acids were mainly produced by a guild consuming lactate. These models represent novel tools for exploring the role of mixed microbial communities on carbon recycling in the environment, as well as on beneficial reuse of organic residues.

INTRODUCTION

Mixed microbial fermentations have benefited humanity throughout history.[1] Since the mid-18th century, mixed culture fermentations have produced food, valuable chemicals, and recovered energy from wastes.[2] Many mixed microbial fermentations involve the synergistic activity of several functional groups to convert organic substrates into valuable products. In anaerobic digestion, fermentation products like acetic acid and H_2 are used to support microbial production of methane, thus enabling the recovery of a large fraction of the chemical energy originally present in the complex organic substrates. While anaerobic digestion technologies are

42 well established, other strategies to expand the range of potential products of mixed culture
43 fermentations are only beginning to emerge, such as the carboxylate platform, which produces
44 medium-chain fatty acids (MCFA) as a potentially valuable set of bio-based products.[3, 4]

45 MCFA are an attractive carboxylate platform product because of their many industrial
46 uses.[5] Octanoic acid (C8), an 8-carbon linear monocarboxylic acid, is a particularly valuable
47 MCFA because of its numerous uses, high market value, and relative ease of recovery. Further,
48 when C8 is reduced to its corresponding alkane, it can substitute for octane in liquid transportation
49 fuels. Recent research has demonstrated the feasibility of using mixed culture fermentations to
50 transform renewable resources into MCFA.[6-8] While C8 is produced in some self-assembled
51 microbial communities that develop in MCFA-producing bioreactors, hexanoic acid (C6) is often
52 the primary MCFA, along with acetic and butyric (C4) acids.[6-13]

53 Mathematical models have been established for the design and optimization of methane
54 production via anaerobic digestion.[14] These models describe the kinetics and stoichiometry of
55 reactions attributed to the individual members of the community that are responsible for hydrolysis
56 of complex organics, the fermentation of hydrolysis products, the transformation of fermentation
57 products to acetic acid and H_2, and finally, the transformation of these intermediates to methane.[14]
58 The metabolic networks in these models are well defined, with interspecies H_2 transfer known to
59 regulate critical metabolic steps, and therefore, anaerobic digestion models are predictive of the
60 behavior of self-assembled methane-producing microbiomes.

61 In contrast, the microbial metabolic networks involved in converting complex organic
62 substrates to MCFA are not fully elucidated. Consequently, there is a lack of knowledge on how
63 to obtain a carboxylate platform microbiome that produces C8 as the main MCFA, or how to
64 minimize the accumulation of shorter-chain fatty acids. Initial models of mixed culture

65 fermentations that do not include methanogenesis have focused on simulating metabolic networks
66 for production of C4, propionic acid, acetic acid, ethanol, lactic acid and H_2 from glucose.[15]
67 Subsequent models took into account that multiple electron carriers (e.g., ferredoxin, NADH) play
68 different roles in these metabolic networks, enabling the simulation of energy-conserving electron-
69 bifurcating reactions during production of C4 by reverse β-oxidation.[16] While a recent model
70 considered the role of homoacetogenesis as a H_2-consuming member of mixed culture
71 fermentation, it was limited to producing C4 as the major MCFA.[17]

72 In addition, existing models of carboxylate platform communities do not test the potential
73 role of recently discovered energy-conserving mechanisms in anaerobic microbes[18] that may shape
74 the metabolic networks of these mixed culture fermentations. Therefore, one goal of this study was
75 to test the ability of different models that considered all the known metabolic networks and energy-
76 conserving mechanisms to predict bottlenecks and strategies to improve MCFA production. To do
77 this, we constructed a single unit model (iFerment156) and a guild-based microbial community
78 model (iFermGuilds564) with expanded capability compared to existing models, and tested their
79 predictive ability using experimental data from a MCFA-producing bioreactor. We used the
80 models to diagnose bottlenecks for improved MCFA production, with particular emphasis on
81 predicting factors and specific enzymes that could alter the amount and type of MCFA produced
82 by the mixed microbial community.

83 **MATERIALS AND METHODS**

84 A metabolic network of a mixed culture fermentation was assembled that contains
85 reactions that occur during anaerobic metabolism of a previously described lignocellulsoic
86 biorefinery residue.[19] The first network, iFerment156, contains 156 reactions and 105 metabolites,
87 models a mixed culture fermentation as a single unit, and expands the metabolic pathways and

88 substrate range of previously published mixed culture fermentation networks.[15-17] iFerment156 is
89 the most comprehensive metabolic model of mixed culture fermentation to date, describing
90 metabolism of exogenous substrates including glucans, glucose, xylans, xylose, and glycerol,
91 along with lactate, ethanol, acetate, CO_2 and H_2, which are potential intermediates in this mixed
92 culture fermentation (**Fig. 1**).

93 The second network, iFermGuilds564, represents activities of different guilds (i.e.,
94 functional classes of organisms) within the microbial community. The iFermGuilds564 network
95 describes the same reactions and metabolites as in the iFerment156 model but these are separated
96 into six functional guilds with each guild representing a subset of compartmentalized reactions.
97 iFermGuilds564 also includes additional transport reactions that simulate metabolite exchange
98 among guilds. Combining the six guilds, the iFermGuilds564 network includes 564 reactions and
99 390 metabolites (**Fig. 2**). The guilds in the iFermGuilds564 model represent previously described
100 organisms that perform fatty acyl chain elongation from sugars (SEOs), sugar fermenting
101 organisms that produce mostly or only lactate, acetate, and ethanol (SFOs) as fermentation
102 products, hydrogenic sugar fermenters (HSFs), organisms that perform fatty acyl chain elongation
103 from lactate (LEOs) or ethanol (EEOs), and homoacetogenic organisms (HAOs). SEOs include
104 organisms that utilize sugars and elongate intermediate products through reverse β-oxidation, such
105 as *Megasphaera* and *Caproicproducens.*[20, 21] SFOs include genera such as *Lactobacillus* and
106 *Bifidobacterium*, which can ferment hexoses and pentoses to lactate, acetate and ethanol.[22, 23] HSFs
107 include organisms that generate H_2 while producing fermentation products, such as members of
108 the *Coriobacteriaceae* family.[24] LEOs include organisms that perform reverse β-oxidation with
109 lactate, such as *Pseudoramibacter*[25] and *Ruminococcaceae* bacterium *CPB6.*[9] EEOs, such as
110 *Clostridium kluyveri,*[26] perform reverse β-oxidation with ethanol. HAOs produce acetate from H_2

111 and CO_2 and include species within the *Clostridium*, *Acetobacterium*, *Eubacterium,* and *Blautia.*[27-
112 29]

113 When constructing each metabolic network, reactions were added to capture the exchange
114 of substrates and products with the reactor (extracellular space).[30] Where possible, standard
115 metabolite and reaction abbreviations from the Biochemical, Genetic, and Genomic (BiGG)
116 knowledgebase were used.[31] All reactions were checked for mass and charge balance assuming an
117 intracellular pH of 7.0 with the dominant ionic form of all metabolites obtained from the BiGG
118 database.[31] Methods for including transport constraints are discussed in **Supplementary Text 1**.
119 Both metabolic models (iFerment156 and iFermGuilds564) are available as **Supplementary File**
120 **1** and **Supplementary File 2**, respectively. Instructions for using the models are available at
121 https://github.com/mscarbor/Mixed-Culture-Fermentation-Models.

122 The production capabilities of both metabolic networks were simulated using constraint-
123 based methods.[32] These methods predict the steady-state flux distribution through a metabolic
124 network that is subject to physiochemical constraints. In this work, we used flux variability
125 analysis (FVA)[33] and parsimonious flux balance analysis (pFBA)[34] to predict flux distributions
126 through metabolic networks of mixed culture fermentation. When modeling bioreactors with the
127 presence of solute gradients across the cell membrane, we considered the ATP required for
128 transport of solutes as described in **Supplementary Text 1.** The objective function for all
129 modeling scenarios was to maximize ATP production. When simulating the iFermGuilds564
130 network for a steady-state condition, we required all individual guilds to achieve the same ATP
131 hydrolysis flux as a proxy for having the same growth rate, as the models do not include biomass
132 equations. All simulations were performed in Python 3.5 using the cobrapy package (v 0.13.4).[35]

133 Throughout this work, we present results in terms of electron equivalents (eeq), which
134 report the number of electrons potentially transferred to an acceptor if the reduced chemical were
135 completely oxidized (using factors provided in **Table S1** to convert from molar concentrations to
136 eeq concentrations). For each scenario, we calculated the overall reaction thermodynamics using
137 the predicted stoichiometry of the model and the standard free energy of formation ($\Delta G_f'^0$) of
138 metabolites (**Supplementary File 3**) obtained from KBase.[36] We ensured that at least 50 kJ was
139 available per ATP produced under standard conditions at neutral pH.[37, 38]

140 **RESULTS**

141 **Simulation of mixed culture fermentations with iFerment156**

142 By constraining the iFerment156 model to produce defined products, we initially tested its
143 predictive ability with well-established fermentation conditions (See **Supplementary Text 2;**
144 **Table S2**). We also investigated predictions derived from an unconstrained iFerment156 model
145 (i.e., all pathways are on) under conditions where multiple substrates are simultaneously produced
146 and consumed within this unit. This modeling analysis is a simplified representation of
147 fermentation in a mixed microbial community where interspecies transfer of metabolites is
148 assumed to have no energetic penalty, and is similar to previously published models of mixed
149 culture fermentations.[15-17] For this analysis, we required that all possible solutions released ≥50 kJ
150 per mol ATP produced as a condition that simulated microbial growth.[37] Using FVA with this
151 condition, iFerment156 provided a range of solutions that maximized ATP production depending
152 on the substrates provided to the simulation (**Fig. 3**). For instance, when we examined the
153 utilization of glucose as the sole substrate, iFerment156 predicted multiple conditions that would
154 allow ATP production at 4.5 mol ATP per mol of glucose metabolized. One of these solutions
155 predicts that 61.1% of the eeq in glucose could be converted to C8 (with 22.2% and 16.7% of the

156 eeq converted to acetate and formate, respectively) (**Fig. 3; Table S3**). Another solution predicts
157 66.6% of the eeq converted to C6, with 16.6% eeq converted to acetate and 16.6% to formate
158 (**Table S3**). Homofermentation to acetate is yet another solution that yields the maximum ATP
159 production. Another prediction from this analysis is that fermentations that result in ethanol or
160 lactate production, although feasible and known to occur in nature, do not result in the maximum
161 possible ATP yields (**Fig. 3**). This prediction of iFerment156 agrees with the practice of using pure
162 cultures (with limited metabolisms) for industrial ethanologenic fermentations, since mixed
163 cultures would likely produce other unwanted fermentation products that help maximize ATP
164 production by the microbial community.

165 The iFerment156 model predicts similar results when xylose is provided as the sole carbon
166 source (**Fig. 3, Table S3**), albeit with a lower ATP production compared to glucose (3.75 mol ATP
167 per mol substrate). We found that providing glycerol as a sole carbon source to iFerment156 yields
168 multiple solutions that maximize ATP production (**Fig. 3**). On the other hand, a single solution
169 that maximizes ATP production is predicted by iFerment156 if either lactate or ethanol are sole
170 carbon sources. When providing lactate, this solution predicts stoichiometric conversion of lactate
171 to C8, while with ethanol, 92% of the eeq would be converted to C8 and 8% to H_2.

172 These results predict that microbial communities would energetically benefit from
173 simultaneously producing multiple fermentation products, which is consistent with experimental
174 observations of fermentation of carbohydrate-rich feedstocks.[6, 8, 39] Consequently, we used
175 iFerment156 to evaluate whether having multiple electron donors simultaneously available would
176 change the predictions of maximum ATP production. In particular, since acetate and H_2 are
177 ubiquitous fermentation products in mixed microbial fermentations, we used iFerment156 to
178 simulate co-utilization of either acetate or H_2 with the other substrates analyzed (**Fig. 3**). With

179 acetate as a co-substrate with glucose, xylose, or glycerol, iFerment156 predicted the same
180 multiple solutions that maximized ATP production in the absence of acetate (**Table S3**). This
181 observation predicts, that from the point of view of maximizing microbial growth, acetate is a final
182 fermentation product. In contrast, co-utilization of lactate and acetate is predicted by iFerment156
183 to increase the ATP yield and favor reverse β-oxidation with solutions that maximize ATP
184 production including butyrate, C6 or C8 production (**Fig. 3; Table S3**). This analysis also found
185 that acetate co-utilization with ethanol is predicted by iFerment156 to double the ATP yield
186 compared to ethanol as the sole carbon source (**Table S3**). In this case, solutions for optimal ATP
187 yields were obtained when butyrate, C6, or C8 were the main fermentation product, consistent
188 with the ability of known carboxylate platform systems to produce a variety of short- and medium-
189 chain products.[40-42] Overall, these iFerment156 simulations suggest that acetate co-utilization can
190 increase the range of accumulated products, but that this may be detrimental to processes targeting
191 production of a single or small set of compounds. Further, these results predict that acetate may be
192 a dead-end product in mixed culture fermentations unless other compounds, such as lactate or
193 ethanol, are either present in the growth substrate or accumulated as intermediates.

194 We also tested the impact of H_2 metabolism on mixed culture fermentation, since this has
195 previously been proposed as either a fermentation intermediate or endogenous reductant to drive
196 MCFA production.[19] During utilization of sugars and glycerol, iFerment156 predicted that the
197 presence of H_2 favors higher ATP yields if C8 is the only fermentation product produced (**Fig. 3**).
198 In the presence of ethanol, H_2 is not predicted to be consumed by iFerment156 since redox balance
199 cannot be maintained under these conditions. In the presence of H_2 and acetate, or H_2 and CO_2, C8
200 production is favored for maximizing ATP production. Thus, iFerment156 predicts that H_2

201 oxidation should improve C8 production because it would maximize the ATP production of the
202 overall microbial community.

203 In sum, iFerment156 can predict substrates that favor accumulation of different products
204 when a large set of biochemical reactions are available in a mixed culture fermentation (**Fig. 1**).
205 When sugars and glycerol are the main substrates, mixed culture fermentations could give rise to
206 a wide range of products since multiple sets of fermentation reactions yield the same maximum
207 ATP production for the community. When lactate or ethanol are the main substrates, a narrower
208 product spectrum may be expected. In addition, H_2 co-utilization may result in accumulation of a
209 narrower range of products from sugars and glycerol as H_2 utilization would increase overall ATP
210 yields. In a large-scale bioreactor, production of fewer products is often considered advantageous
211 for downstream processing and to improve overall process economics.

212 **Simulation of bioreactor performance with a single-unit model (iFerment156)**

213 The iFerment156 model predicts that multiple substrates could lead to C8 production (**Fig.**
214 **3**), but that ATP could be maximized by co-production of other fermentation products. We wanted
215 to assess if this single-unit model could simulate the observed product yields of a bioreactor fed
216 lignocellulosic biorefinery residues, a complex organic substrate.[19] The microbial community in
217 the bioreactor (derived from wastewater sludge) was fed lignocellulosic biorefinery residues for
218 96 days, at which time bioreactor performance was evaluated using metagenomic and
219 metatranscriptomic analyses along with end-product sampling.[19] At this time, the bioreactor
220 contained 11.7 g L^{-1} of volatile suspended solids, which was assumed to represent microbial
221 biomass. To represent organic substrate metabolism, the substrate uptake fluxes were set according
222 to the eeq consumed for compounds in the feedstock (**Table S4**). We constrained iFerment156 to
223 only contain reactions predicted by transcriptomic analyses to be active in the bioreactor microbial

224 community[19] and performed FVA to identify the range of end-products that would support
225 maximum ATP yields. Under these conditions, iFerment156 predicted that 90% of the eeq would
226 be converted to C8 (**Fig. 4A**), which is much higher than the 3% conversion to C8 observed in the
227 bioreactor. The total predicted ATP production rate is 1.37 mmol hr^{-1}. While this simulation of
228 iFerment156 did not correctly predict the range of products (butyrate, C6 and C8) measured in the
229 bioreactor, it did indicate that C8 production could be advantageous for maximizing ATP
230 production.

231 Because C6 and C8 are known biocides,[43, 44] it is possible that their production is limited
232 by their accumulation. To test this hypothesis, we performed simulations constraining this version
233 of iFerment156 to produce C6 and C8 at the rates measured in the bioreactor (**Table S3**). Using
234 these parameters, iFerment156 predicted an ATP production rate of 1.32 mmol hr^{-1} (**Fig. 4B**),
235 corresponding to 96% of the maximum ATP production rate predicted when C6 and C8 production
236 were not constrained. Under these conditions, iFerment156 predicted that 50% of the eeq were
237 converted to butyrate, approximately 1.5-fold higher than was observed in the bioreactor (34% of
238 the eeq, **Fig. 4B**). Although the discrepancies between predicted and measured MCFA levels
239 indicate limitations in the ability of iFerment156 to predict performance of this mixed microbial
240 community, the similar ATP yield predictions when the model was constrained to the observed C6
241 and C8 concentrations illustrates the difficulty of simulating the sum of all metabolic processes
242 with a single-unit model. However, energetic losses associated with interspecies transfer of
243 substrates may influence the predicted ATP yields and the resulting levels of fermentation
244 products. To investigate this, a functional guild fermentation model was developed, based on the
245 reactions present in iFerment156, as described in the next section.

246 **Simulation of mixed culture fermentations with a functional guild model (iFermGuilds564)**

247 In iFermGuilds564, the metabolic activities of a microbial community are partitioned
248 among a number of functional guilds. This biological division of labor negates the free exchange
249 of reducing equivalents (e.g., NADH, ferredoxin) and of many pathway intermediates (e.g., acetyl-
250 CoA) between community members, ultimately constraining how individual organisms maintain
251 redox balance, which can potentially impact ATP and product yields. For instance, the single unit
252 model (iFerment156) cannot predict the production of lactate via a NADH-dependent
253 dehydrogenase and re-consumption of lactate via an electron-confurcating dehydrogenase,
254 activities that may happen in a microbial community that includes lactate producers and lactate
255 consumers. Thus, to better represent the compartmentalized nature of microbial activities within
256 microbiomes we developed a functional guild model (iFermGuilds564) to simulate mixed culture
257 fermentations where community members exchange extracellular intermediates. The
258 iFermGuilds564 model contains the fermentation pathways in six guilds (**Fig. 2**), with each guild
259 including predictions on transport reactions to simulate uptake and release of intermediate
260 metabolites.

261 Initial predictions with iFermGuilds564 were focused at evaluating the role of each
262 community member on the performance of this mixed culture fermentation. First, we used
263 iFermGuilds564 to predict the fermentation of glucose by each of the guilds individually (**Table**
264 **1)** using an approach similar to that used with the iFerment156 model. That is, we required a
265 release of ≥50 kJ per mol ATP produced as a condition that simulated microbial growth. As
266 expected, only the guilds with reactions needed to degrade carbohydrates were predicted to
267 produce ATP under these conditions. Specifically, iFermGuilds564 predicted that **s**ugar-
268 elongating organisms (SEOs) are predicted to have the highest ATP yield and produce C8, CO_2,

269 and H_2 (**Table 1**). In addition, sugar-fermenting organisms (SFOs) are predicted by
270 iFermGuilds564 to produce both acetate and lactate, but not CO_2. In contrast, iFermGuilds564
271 predicts that HSFs have a higher ATP yield than SFOs and produce acetate, ethanol CO_2, and H_2,
272 while no growth was predicted for several guilds that represent other major members of the mixed
273 microbial community (**Table 1**). In total, simulations of these individual guilds show that they
274 vary in the amount of ATP that can be produced from the same substrate. In addition, these
275 simulations predict that all of the guilds produce less ATP than a single organism containing all of
276 these reactions (iFerment156, 4.5 mol ATP mol^{-1} glucose, **Fig. 3**).

277 **Table 1.** iFermGuilds564 predicted overall chemical reactions, ATP yields, thermodynamics, and carbon
278 capture by individual guilds fed glucose.

Functional Guild	Predicted Reaction	ATP Yield	$\Delta G^{0'}$ mol^{-1} ATP	Carbon Capture
SEOs	$C_6H_{12}O_6 \rightarrow 0.5\ C_8H_{15}O_2^- + H_2O + H_2 + 0.5\ H^+ + 2\ CO_2$	4.0	-69.3	66.7%
SFOs	$C_6H_{12}O_6 \rightarrow C_3H_5O_3^- + 1.5\ C_2H_3O_2^- + 2.5\ H^+$	2.5	-74.1	100%
HSFs	$C_6H_{12}O_6 + 0.5H_2O \rightarrow 2C_2H_6O_3^- + 0.5C_2H_6O + H_2 + 2H^+ + CO_2$	3.0	-87.9	83.3%
LEOs	*No Growth Predicted*			
EEOs	*No Growth Predicted*			
HAOs	*No Growth Predicted*			

279

280 To explore whether iFermGuilds564 would better simulate the experimental observations
281 in the MCFA-producing bioreactor, compared to iFerment156 (**Fig. 4**), we used a version of
282 iFermGuild564 with only four guilds, which represented the most abundant community members
283 in the bioreactor as determined by metagenome sequencing,[19] which were a *Lachnospiraceae*
284 (SEO guild), *Eubacteriaceae* (LEO guild), *Lactobacillus* (SFO guild), and *Coriobacteriaceae*
285 (HSF guild). Performance of these guilds were simulated with substrate constraints that were based

286 on a combination of experimental observations and predictions from previous metabolic network
287 reconstructions[19]: SEOs were constrained to use glucose, xylose and glycerol. SFOs could
288 consume glucose, xylose, xylans, glucans, and glycerol whereas HSFs were constrained to only
289 consume glucans, glucose and glycerol, and LEOs were restricted to consuming only lactate and
290 glycerol (**Table S5**).

291 To mimic steady-state bioreactor conditions, we constrained each iFermGuilds564 model
292 so that specific ATP production rates (mmol ATP $gDCW^{-1}$ hr^{-1}) for each guild were equal, assumed
293 that the guilds were present according to their measured relative DNA abundance,[19] and performed
294 FVA optimizing for the overall ATP production rate of the community. Under these conditions,
295 iFermGuilds564 had multiple solutions that predicted a maximum ATP rate of 0.58 mmol ATP hr^{-}
296 ^{1}. The solutions derived from these iFermGuilds564 simulations predict that a range of products
297 could be produced while maintaining the maximum ATP yield (**Fig. 4C**). This is different from
298 the predictions derived from the iFerment156 model, where single solutions were found that
299 maximized ATP yield (**Fig. 4A**). However, both iFerment156 and iFermGuilds564 predict that
300 maximum ATP yields would be attained if C8 is produced from organics in conversion residue
301 and they overpredict the percent of eeq that is required to be converted to C8 when compared to
302 experimental data (30-90%, **Fig. 4C**).

303 Constraining the iFermGuilds564 simulation of the above four guilds to produce C6 and
304 C8 based on their observed production in the bioreactor (**Fig. 4D**), improved its predictions, with
305 only a minor reduction in the predicted rate of ATP production (i.e., 0.57 mol ATP hr^{-1}, ~99% of
306 the maximum ATP yield predicted when C6 and C8 production was not constrained). This finding
307 supports the notion that toxicity of individual MFCAs may impact the observed product
308 composition and that the energetic cost of reduced C8 production is minimal. In these simulations,

309 the predicted levels of other end-products using iFermGuilds564 were better aligned with those
310 observed in a bioreactor that is fed with the lignocellulosic biorefinery residues (**Fig. 4D**).

311 The predicted ATP production rates of 1.32-1.37 mmol ATP hr^{-1} with iFerment156 (**Figs.**
312 **4A and 4B**) are about two-fold higher than the 0.57-0.58 mmol ATP hr^{-1} predicted in
313 iFermGuilds564 when the reaction sets are compartmentalized in functional guilds. This suggests
314 that compartmentalization of reaction sets into individual guilds (microbes) greatly influences ATP
315 production by mixed culture fermentation communities. Therefore, our analysis predicts that
316 functional guild metabolic models have advantages over unicellular models for assessing the
317 performance of mixed microbial communities like those in a carboxylate platform bioreactor.

318 **Assessing interspecies metabolite flux using iFermGuilds546**

319 Our previous data predict that the individual microbes within the MCFA-producing
320 microbial community perform different functions, compete for resources, and participate in the
321 interspecies transfer of metabolites that ultimately allows the lignocellulosic biorefinery residues
322 to be converted to short- and medium-chain fatty acids. Based on this, we sought to use
323 iFermGuilds564 to test our ability to model the predicted function of each guild in the
324 transformation of substrates as well as the production and transfer of intermediate metabolites
325 between microbes. For this, we constrained iFermGuilds564 to produce end-products at the rates
326 observed in the MCFA-producing bioreactor (**Table S3**), set the substrates consumed by each guild
327 as described above, and predicted fluxes using pFBA which calculates a single flux distribution
328 when the model is constrained to the observed end-product production rates. Under these
329 conditions, iFermGuilds564 predicted a production rate of 0.54 mmol ATP hr^{-1}, which is 93% of
330 the maximum ATP production rate derived from the FVA analysis (**Fig. 4C**). The agreement of

331 the predicted ATP production rates by these methods suggests that, as a whole, the bioreactor
332 community is functioning near its optimal growth rate.

333 Under these conditions, iFermGuilds564 predicted that the glycerol would be consumed
334 by SEOs, xylose consumption would be shared by SEOs and SFOs, glucose would exclusively be
335 consumed by HSFs, glucans consumed by SFOs and HSFs, and xylans exclusively consumed by
336 SFOs (**Fig. 5**). In addition, these iFermGuilds564 simulations predicted that SEOs would produce
337 all the C8, most of the C6, and some H_2; SFOs were predicted to perform homofermentative lactate
338 production; HSFs were predicted to perform heterofementative production of lactate, acetate,
339 ethanol, and H_2; LEOs were the predicted lactate consumers who produced a combination of
340 acetate, butyrate, C6 and H_2. When we modeled how the H_2 partial pressure might impact the
341 predicted conversion routes, a thermodynamic analysis of each guild indicates that these predicted
342 reactions are feasible at both high and low H_2 partial pressures (**Table 2**). Thus, these
343 iFermGuilds564 simulations indicated that, unlike conventional anaerobic digestion, MCFA
344 production via mixed culture fermentation may proceed under a wide range of H_2 partial pressures.

345 **Table 2.** Thermodynamics of the net chemical reactions for each functional guild. ΔG' values are calculated
346 at neutral pH at the noted H_2 partial pressures assuming all other compound concentrations are present at 1
347 mM.

Functional Guild	Reactor Population Name	Relative Abundance	Transport - associated ATP (mmol hr^{-1})	Growth - associated ATP (mmol hr^{-1})	Total ATP Production (mmol hr^{-1})	ΔG' mol^{-1} ATP	
						P_{H2} = 1 atm	P_{H2} = 10^{-3} atm
SEO	*Lachnospiraceae*	45%	0.00766	0.243	0.250	-67.5	-75.5
SFO	*Lactobacillus*	40%	0.00	0.216	0.216	-73.8	-73.8
HSF	*Coriobacteriaceae*	10%	0.00143	0.0539	0.0554	-81.0	-83.0
LEO	*Eubacteriaceae*	5%	0.0390	0.0270	0.0660	-146	-163

348

349 These iFermGuilds564 simulations also predicted that lactate was the only product that
350 was re-consumed by the community. This prediction suggests that acetate and butyrate are

351 undesirable fermentation end-products if the goal is to maximize C6 or C8 production in the
352 bioreactor.

353 An additional prediction of iFermGuilds564is that LEOs, which only represented 5% of
354 the microbial community, were predicted to produce 72% of the H_2, 87% of the acetate, 100% of
355 the butyrate and no significant quantities of C6 and C8 (**Fig. 5A**). This predicted flux of lactate to
356 end-products that do not contribute to MCFA production suggests that LEOs could be a potential
357 bottleneck for high levels of MCFA production. This prediction is in apparent contradiction with
358 those from the iFerment156 simulations (**Fig. 3**) that suggested maximization of ATP production
359 would occur if C8 is the final product of lactate utilization. One possible explanation for this
360 discrepancy is that LEOs are growing at sub-optimal conditions in the bioreactor given the
361 imposed restrictions on growth rate (see below).

362 **Predicted metabolic efficiency of guilds in a MCFA-producing bioreactor**

363 The previous simulations with iFermGuilds564 assumed that the specific ATP production
364 rates (mmol ATP $gDCW^{-1}$ hr^{-1}) for each guild were equal. This constraint was imposed to simulate
365 observed steady-state bioreactor conditions where the relative concentration of each guild remains
366 constant over time. However, the previous iFermGuilds564 simulations did not consider potential
367 variations in maintenance energy requirements across the different guilds. Since we lack pure
368 cultures of the organisms in the bioreactor, we used the metabolic models to estimate the efficiency
369 of ATP production for each guild within the reactor community. To do this, we constrained the
370 individual guild models to consume the substrates that they are predicted to metabolize in the
371 mixed culture community (**Fig 5**). Under these conditions, and in the absence of competition for
372 substrate or restrictions of needing to have a common specific ATP production rate for all the
373 guilds, we allowed the iFermGuilds564 simulation to predict the maximum yield of ATP used for

374 growth (**Table 3**). An ATP production efficiency was then calculated based on a comparing the
375 predicted growth-associated ATP production in the iFermGuilds564 model and the maximum ATP
376 yield in the single unit iFerment156 simulation (**Table 3**). The predicted ATP production
377 efficiencies of guilds vary widely from SEOs (96.4%) and SFOs (95.6%) to LEOs (14.1%) (**Table**
378 **3**). This result predicts that LEOs grow at sub-optimal conditions in the bioreactor where there is
379 no selective pressure for them to produce MCFA over shorter chain organic acids or other products.

380 **Table 3. Predicted ATP production efficiency of each guild modeled in the bioreactor.**

Guild	Predicted Growth ATP with iFermGuilds564 (mmol hr^{-1})	Maximum predicted Growth ATP (mmol hr^{-1})	Efficiency (%)
SEOs	0.244	0.253	96.4%
SFOs	0.217	0.227	95.6%
HSFs	0.054	0.067	80.6%
LEOs	0.027	0.191	14.1%
LEOs[1]	0.027	0.064	42.4%

381 [1]LEOs constrained to use electron confurcating lactate dehydrogenase exclusively

382 Another explanation for these findings is that the metabolic networks used in the simulation
383 of LEOs are not correct, causing the model to overpredict ATP production by this guild. In order
384 to test this hypothesis, we evaluated an alternative route for lactate metabolism in LEOs. That is,
385 LEOs were initially modeled as using two different lactate dehydrogenases for the transformation
386 of lactate to pyruvate, a NADH-dependent lactate dehydrogenase (LDH) and an electron
387 confurcating lactate dehydrogenase (ECLDH), in which lactate transformation is coupled to
388 ferredoxin oxidation as described for the anaerobic lactate-consuming *Acetobacterium woodii*.[45]
389 With these assumptions, the iFermGuilds564 simulation of the LEOs indicated preferential use of
390 LDH over ECLDH (**Fig. S1A**). Thus, we also ran simulations in which the LEOs exclusively use
391 ECLDH (**Fig. S1B**). We found that, if LEOs are forced to use ECLDH, their maximum predicted
392 ATP production drops from 0.191 to 0.0637 mmol ATP hr^{-1}, predicting an efficiency of 42.4% in
393 the bioreactor, rather than 14.1% (**Table 3**). While this scenario results in an improvement in the

394 prediction, it suggests that use of ECLDH alone does not fully explain the inefficiencies of LEOs.
395 In scenarios where the LEOs exclusive using ECLDH for lactate metabolism, the simulations
396 predict that the overall flow of carbon through the community is nearly identical to those in other
397 simulations (**Supplementary File 4**). In addition, while the overall ATP production rate for the
398 community remains at 0.54 mmol ATP hr^{-1} when lactate is metabolized by ECLDH but the
399 predicted energy metabolism of LEOs changes in several ways (**Supplementary Text 3)**.

400 In sum, simulating the bioreactor community with iFermGuilds564 suggests that SEOs are
401 responsible for producing C8 in the bioreactor. While the model of LEOs contain all of the
402 reactions necessary for producing C8, these microbes are predicted to produce most of the acetate,
403 butyrate and H_2 in the bioreactor. LEOs are predicted to have low growth efficiencies and may
404 require large amounts of ATP for processes other than growth and transport. While the inclusion
405 of ECLDH results in a higher overall energetic efficiency for LEOs (42.4%), this is still lower than
406 the predicted efficiencies of the other guilds in the mixed microbial community (**Table 3**).
407 Combined these predictions suggest that LEOs use ECLDH and may have other ATP-consuming
408 processes not currently captured by the metabolic model. The iFermGuilds564 predictions also
409 suggest that SEOs are a better source for MCFA production than LEOs when fed a carbohydrate-
410 rich substrate. Further, H_2 and acetate were always predicted to be metabolic end-products rather
411 than intermediates in MCFA production, suggesting that acetate is not a productive intermediate
412 in MCFA production by this community and that electron transfer between species could be
413 improved to alter the suite of desired products.

414 **Improved MCFA production by a mixed microbial community**

415 The predictions derived from metabolic models like iFermGuilds564 could also help guide
416 the engineering of natural or synthetic communities that convert complex organic residues to a

417 desired set of products. While a reactor containing only SEOs is predicted by iFermGuilds564 to
418 favor C8 production (**Supplementary File 4**), 26% of the carbon from these organisms is predicted
419 to be lost as CO_2. To test if a synthetic microbial community could convert 100% of the carbon
420 and eeq to C8 when fed lignocellulosic biorefinery residues, we used iFermGuilds564 to assemble
421 an *in silico* community to convert all of the carbon in this feedstock to C8. To limit carbon loss as
422 CO_2 by the SEOs, we included HAOs in this synthetic community and simulated the addition of
423 an external electron donor, H_2, to drive homoacetogenic activity to convert endogenous CO_2 to
424 acetate that could undergo chain elongation. We tested the performance of this synthetic
425 community, under various conditions, including different ratios of each microbe, partial pressures
426 of H_2 and others.

427 One synthetic community that was predicted to convert all of the eeq in lignocellulosic
428 biorefinery residues and exogenous H_2 to C8 contained 90% SEOs and 10% HAOs, both of which
429 were predicted to both use exogenous H_2 (**Fig. 6**). In this modeled synthetic community, HAOs
430 were predicted to use H_2 to fix CO_2 produced by SEOs, and acetate produced by the HAOs was a
431 major source for chain elongation by the SEOs. Formate produced by SEOs would also be used
432 by the HAOs as a source of carbon and reducing power. Analyzing the scenarios predicted for
433 each guild indicate that a H_2 partial pressure $\leq 10^{-6}$ atm would make the predicted ATP produced
434 by HAOs thermodynamically infeasible. However, at H_2 partial pressures $\geq 10^{-3}$ atm, the
435 transformations and predicted ATP yields of the two-guild mixed culture fermentation were
436 sufficient to support C8 production (**Table 4**). Further, metabolic modeling of this synthetic
437 community predicts that increased C8 production could be achieved if HAOs could more readily
438 utilize H_2 that is produced or provided to the reactor.
439

440

441

442 **Table 4.** Predicted thermodynamics of a synthetic community of SEOs and HAOs converting conversion

443 residue and H_2 to C8.

Functional Guild	Relative Abundance	Predicted ATP Production (mol hr^{-1})	ΔG' mol^{-1} ATP	
			P_{H2} = 1 atm	P_{H2} = 10^{-3} atm
SEO	90%	0.728	-100	-87.6
HAO	10%	0.081	-160	-86.8
Total		0.809	-106	-87.6

444

445 **DISCUSSION**

446 Under anaerobic conditions, a diverse set of mixed microbial communities catalyze the
447 transformation of organic substrates to a variety of products. Some fermentation metabolisms are
448 well understood, using genetically tractable pure cultures that can be analyzed, modeled and
449 improved for use in industrial applications.[46, 47] For over a century, anaerobic microbial
450 communities have been harnessed to recover energy, in the form of methane-rich biogas, from
451 complex organic matter in anaerobic digestion.[2] The ability to harness the metabolic activity of
452 mixed microbial communities to produce alternative fermentation products is limited since
453 metabolic and kinetic models that accurately predict the distribution of fermentation products are
454 only starting to emerge.[15-17] To address this knowledge gap, we constructed metabolic models of
455 mixed culture fermentations with the objective of gaining greater insights into how to increase
456 MCFA production by mixed microbial communities. We focused on producing C6 and C8, linear
457 medium-length MCFA of industrial value that can be produced from a variety of organic residues.[3]

458 Since many microbes in self-assembled fermentation communities remain uncultured, our
459 knowledge and ability to predict important metabolic networks of these mixed cultures relies
460 largely on information from metagenomics, metatranscriptomics and metabolomics analyses to

461 build the functional activities in each guild.[19, 48] We show in this work that metabolic modeling
462 offers additional insight that is not gained by these analyses, but that is critical in their evaluation
463 and in developing hypothesis of how to direct metabolism towards a specific set of fermentation
464 products. For instance, while iFermGuilds564 included three guilds capable of MCFA production
465 (SEOs, LEOs, and EEOs; **Fig. 2**), only SEOs and LEOs were included in many simulations since
466 reactor performance did not indicate ethanol as a fermentation product.[19] From prior analyses[19, 49]
467 we anticipated that both SEOs and LEOs participated in MCFA production, but the
468 iFermGuilds564 simulation of interspecies metabolite flux (**Fig. 5**) predicted that, to maximize the
469 overall ATP production in the community, C8 was largely produced by SEOs, while LEOs were
470 responsible for production of butyrate and acetate as fermentation end-products that were not
471 converted to MCFA. This finding makes the unexpected prediction that minimizing the abundance
472 or activity of LEOs would maximize MCFA production by this community.

473 We further showed that a guilds-based fermentation model such as iFermGuilds564 can be
474 used to evaluate scenarios for how to direct a mixed microbial community to produce specific
475 fermentation products from more efficient utilization of complex organic substrates (**Fig. 6**). For
476 example, iFerment156 predicted that H_2 is both a product during MCFA production (**Fig. 5**) and a
477 source of reducing power that could maximize MCFA production by simplifying the range of
478 accumulated fermentation products (**Fig. 3**). In addition, the results of this simulation predict a
479 previously unrealized role of HAOs, a guild that is not abundant in bioreactors transforming
480 lignocellulosic biorefinery residues to MCFA,[6, 19] but that could be enriched by an exogenous
481 supply of H_2 (**Fig. 6**). The use of metabolic models to assemble an ideal microbial community
482 represents an important new step to bioprocess design that include synthetic or self-assembled
483 communities optimized through the application of selective pressures such as H_2 supply.

484 iFerment156 and iFermGuilds564 are examples of first-generation predictive models of
485 mixed culture fermentations. Their utility can be improved by obtaining additional knowledge of
486 metabolic pathways in individual microbes and genetic studies to test predictions of the metabolic
487 potential of the community members that compliment multi-omic analyses. Further effort is
488 needed to simulate poorly appreciated conditions that shape community structure, such as the
489 toxicity of fermentation products on the specific guilds or the contribution(s) of low abundance
490 microbes to the overall activity of the mixed culture fermentation. Additionally, ours and many
491 models are limited to maximizing community ATP production as a proxy for microbial growth, so
492 computational methods to predict the abundance of specific guilds, rather than relying on relative
493 abundances as a model input, are needed. Efforts to assemble such models have begun for the
494 human gut microbiome,[50, 51] and as these approaches are applied to mixed microbial fermentations,
495 their benefits to the production of MCFA and other chemicals of societal importance will continue
496 to improve.

497 **ACKNOWLEDGMENTS**

498 This work was funded by the DOE Great Lakes Bioenergy Research Center (DOE BER
499 Office of Science DE-SC0018409). M.J.S. was supported by the National Science Foundation
500 Graduate Research Fellowship Program under grant No. DGE-1256259. JJH was supported by the
501 National Institute of Food and Agriculture, U.S. Department of Agriculture, under award number
502 2016-67012-24709. The authors extend our gratitude to Robert Aidan Campbell for assistance
503 with python coding.

504 **REFERENCES**

505 1. McGovern, P. E.; Zhang, J.; Tang, J.; Zhang, Z.; Hall, G. R.; Moreau, R. A.; Nunez, A.;
506 Butrym, E. D.; Richards, M. P.; Wang, C. S.; Cheng, G.; Zhao, Z.; Wang, C., Fermented beverages
507 of pre- and proto-historic China. *Proc. Natl. Acad. Sci. U. S. A.* **2004,** *101*, (51), 17593-8.

508 2. Bond, T.; Templeton, M. R., History and future of domestic biogas plants in the developing
509 world. *Energy for Sustainable Development* **2011,** *15*, (4), 347-354.

510 3. Angenent, L. T.; Richter, H.; Buckel, W.; Spirito, C. M.; Steinbusch, K. J. J.; Plugge, C.
511 M.; Strik, D.; Grootscholten, T. I. M.; Buisman, C. J. N.; Hamelers, H. V. M., Chain Elongation
512 with Reactor Microbiomes: Open-Culture Biotechnology To Produce Biochemicals. *Environ. Sci.*
513 *Technol.* **2016,** *50*, (6), 2796-2810.

514 4. Chen, W. S.; Strik, D.; Buisman, C. J. N.; Kroeze, C., Production of Caproic Acid from
515 Mixed Organic Waste: An Environmental Life Cycle Perspective. *Environ. Sci. Technol.* **2017,**
516 *51*, (12), 7159-7168.

517 5. Sarria, S.; Kruyer, N. S.; Peralta-Yahya, P., Microbial synthesis of medium-chain
518 chemicals from renewables. *Nat. Biotechnol.* **2017,** *35*, (12), 1158-1166.

519 6. Scarborough, M. J.; Lynch, G.; Dickson, M.; McGee, M.; Donohue, T. J.; Noguera, D. R.,
520 Increasing the economic value of lignocellulosic stillage through medium-chain fatty acid
521 production. *Biotechnology for Biofuels* **2018,** *11*, (1), 200.

522 7. Nelson, R.; Peterson, D.; Karp, E.; Beckham, G.; Salvachúa, D., Mixed Carboxylic Acid
523 Production by Megasphaera elsdenii from Glucose and Lignocellulosic Hydrolysate. *Fermentation*
524 **2017,** *3*, (1), 10.

525 8. Kucek, L. A.; Xu, J. J.; Nguyen, M.; Angenent, L. T., Waste Conversion into n-Caprylate
526 and n-Caproate: Resource Recovery from Wine Lees Using Anaerobic Reactor Microbiomes and
527 In-line Extraction. *Front. Microbiol.* **2016,** *7*.

528 9. Zhu, X.; Zhou, Y.; Wang, Y.; Wu, T.; Li, X.; Li, D.; Tao, Y., Production of high-
529 concentration n-caproic acid from lactate through fermentation using a newly isolated
530 Ruminococcaceae bacterium CPB6. *Biotechnol Biofuels* **2017,** *10*, 102.

531 10. Kucek, L. A.; Nguyen, M.; Angenent, L. T., Conversion of L-lactate into n-caproate by a
532 continuously fed reactor microbiome. *Water Res.* **2016,** *93*, 163-171.

533 11. Coma, M.; Vilchez-Vargas, R.; Roume, H.; Jauregui, R.; Pieper, D. H.; Rabaey, K.,
534 Product Diversity Linked to Substrate Usage in Chain Elongation by Mixed-Culture Fermentation.
535 *Environ. Sci. Technol.* **2016,** *50*, (12), 6467-76.

536 12. Spirito, C. M.; Marzilli, A. M.; Angenent, L. T., Higher Substrate Ratios of Ethanol to
537 Acetate Steered Chain Elongation toward n-Caprylate in a Bioreactor with Product Extraction.
538 *Environ. Sci. Technol.* **2018,** *52*, (22), 13438-13447.

539 13. Ge, S.; Usack, J. G.; Spirito, C. M.; Angenent, L. T., Long-Term n-Caproic Acid
540 Production from Yeast-Fermentation Beer in an Anaerobic Bioreactor with Continuous Product
541 Extraction. *Environ. Sci. Technol.* **2015,** *49*, (13), 8012-21.

542 14. Batstone, D. J.; Keller, J.; Angelidaki, I.; Kalyuznyi, S. V.; Pavlostathis, S. G.; Rozzi, A.;
543 Sanders, W. T. M.; Siegrist, H.; Vavilin, V. A., The IWA Anaerobic Digestion Model No 1
544 (ADM1). *Water Sci. Technol.* **2002,** *45*, (10), 65-73.

545 15. Rodriguez, J.; Kleerebezem, R.; Lema, J. M.; van Loosdrecht, M. C. M., Modeling product
546 formation in anaerobic mixed culture fermentations. *Biotechnol. Bioeng.* **2006,** *93*, (3), 592-606.

547 16. Zhang, F.; Zhang, Y.; Chen, M.; van Loosdrecht, M. C. M.; Zeng, R. J., A modified
548 metabolic model for mixed culture fermentation with energy conserving electron bifurcation
549 reaction and metabolite transport energy. *Biotechnol. Bioeng.* **2013,** *110*, (7), 1884-1894.

550 17. Regueira, A.; Gonzalez-Cabaleiro, R.; Ofiteru, I. D.; Rodriguez, J.; Lema, J. M., Electron
551 bifurcation mechanism and homoacetogenesis explain products yields in mixed culture anaerobic
552 fermentations. *Water Res.* **2018,** *141*, 349-356.

553 18. Buckel, W.; Thauer, R. K., Flavin-Based Electron Bifurcation, Ferredoxin, Flavodoxin,
554 and Anaerobic Respiration With Protons (Ech) or NAD(+) (Rnf) as Electron Acceptors: A
555 Historical Review. *Front. Microbiol.* **2018,** *9*, 401.

556 19. Scarborough, M. J.; Lawson, C. E.; Hamilton, J. J.; Donohue, T. J.; Noguera, D. R.,
557 Metatranscriptomic and thermodynamic insights into medium-chain fatty acid production using
558 an anaerobic microbiome. *mSystems* **2018**.

559 20. Marounek, M.; Fliegrova, K.; Bartos, S., Metabolism and Some Characteristics of Ruminal
560 Strains of Megasphaera-Elsdenii. *Appl. Environ. Microbiol.* **1989,** *55*, (6), 1570-1573.

561 21. Kim, B. C.; Seung Jeon, B.; Kim, S.; Kim, H.; Um, Y.; Sang, B. I., Caproiciproducens
562 galactitolivorans gen. nov., sp. nov., a bacterium capable of producing caproic acid from galactitol,
563 isolated from a wastewater treatment plant. *Int. J. Syst. Evol. Microbiol.* **2015,** *65*, (12), 4902-8.

564 22. Ganzle, M. G.; Follador, R., Metabolism of oligosaccharides and starch in lactobacilli: a
565 review. *Front. Microbiol.* **2012,** *3*, 340.

566 23. Kandler, O., Carbohydrate metabolism in lactic acid bacteria. *Antonie Van Leeuwenhoek*
567 **1983,** *49*, (3), 209-24.

568 24. Dewhirst, F. E.; Paster, B. J.; Tzellas, N.; Coleman, B.; Downes, J.; Spratt, D. A.; Wade,
569 W. G., Characterization of novel human oral isolates and cloned 16S rDNA sequences that fall in
570 the family Coriobacteriaceae: description of olsenella gen. nov., reclassification of Lactobacillus
571 uli as Olsenella uli comb. nov. and description of Olsenella profusa sp. nov. *Int. J. Syst. Evol.*
572 *Microbiol.* **2001,** *51*, (Pt 5), 1797-804.

573 25. Holdeman, L. V.; Elizabeth, C. P.; Moore, W. E. C., Amended description of
574 Ramibacterium alactolyticum Prevot and Taffanel with propoosal of a neotype strain. *Int. J. Syst.*
575 *Bacteriol.* **1967,** *17*, (4), 323-341.

576 26. H. A. Barker, M. D. K., and B.T. Borenson, The synthesis of butyric and caproic acid from
577 ethanol and acetate by Clostridium
578 Kluyveri. *Proc. Natl. Acad. Sci. U. S. A.* **1945,** *31*, (12), 374-381.

579 27. Henderson, G.; Naylor, G. E.; Leahy, S. C.; Janssen, P. H., Presence of Novel, Potentially
580 Homoacetogenic Bacteria in the Rumen as Determined by Analysis of Formyltetrahydrofolate
581 Synthetase Sequences from Ruminants. *Appl. Environ. Microbiol.* **2010,** *76*, (7), 2058-2066.

582 28. Hugenholtz, J.; Ljungdahl, L. G., Metabolism and energy generation in homoacetogenic
583 clostridia. *FEMS Microbiol. Rev.* **1990,** *7*, (3-4), 383-9.

584 29. Balch, W. E.; Schoberth, S.; Tanner, R. S.; Wolfe, R. S., Acetobacterium, a New Genus of
585 Hydrogen-Oxidizing, Carbon Dioxide-Reducing, Anaerobic Bacteria. *Int. J. Syst. Bacteriol.* **1977,**
586 *27*, (4), 355-361.

587 30. Covert, M. W.; Schilling, C. H.; Famili, I.; Edwards, J. S.; Goryanin, I. I.; Selkov, E.;
588 Palsson, B. O., Metabolic modeling of microbial strains in silico. *Trends Biochem. Sci.* **2001,** *26*,
589 (3), 179-186.

590 31. King, Z. A.; Lu, J.; Drager, A.; Miller, P.; Federowicz, S.; Lerman, J. A.; Ebrahim, A.;
591 Palsson, B. O.; Lewis, N. E., BiGG Models: A platform for integrating, standardizing and sharing
592 genome-scale models. *Nucleic Acids Res.* **2016,** *44*, (D1), D515-22.

593 32. Bordbar, A.; Monk, J. M.; King, Z. A.; Palsson, B. O., Constraint-based models predict
594 metabolic and associated cellular functions. *Nat. Rev. Genet.* **2014,** *15*, (2), 107-20.

595 33. Gudmundsson, S.; Thiele, I., Computationally efficient flux variability analysis. *BMC*
596 *Bioinformatics* **2010,** *11*, 489.

597 34. Lewis, N. E.; Hixson, K. K.; Conrad, T. M.; Lerman, J. A.; Charusanti, P.; Polpitiya, A.
598 D.; Adkins, J. N.; Schramm, G.; Purvine, S. O.; Lopez-Ferrer, D.; Weitz, K. K.; Eils, R.; Konig,
599 R.; Smith, R. D.; Palsson, B. O., Omic data from evolved E-coli are consistent with computed
600 optimal growth from genome-scale models. *Mol. Syst. Biol.* **2010,** *6*.

601 35. Ebrahim, A.; Lerman, J. A.; Palsson, B. O.; Hyduke, D. R., COBRApy: COnstraints-Based
602 Reconstruction and Analysis for Python. *BMC Syst. Biol.* **2013,** *7*, 74.

603 36. Arkin, A. P.; Cottingham, R. W.; Henry, C. S.; Harris, N. L.; Stevens, R. L.; Maslov, S.;
604 Dehal, P.; Ware, D.; Perez, F.; Canon, S.; Sneddon, M. W.; Henderson, M. L.; Riehl, W. J.;
605 Murphy-Olson, D.; Chan, S. Y.; Kamimura, R. T.; Kumari, S.; Drake, M. M.; Brettin, T. S.; Glass,
606 E. M.; Chivian, D.; Gunter, D.; Weston, D. J.; Allen, B. H.; Baumohl, J.; Best, A. A.; Bowen, B.;
607 Brenner, S. E.; Bun, C. C.; Chandonia, J. M.; Chia, J. M.; Colasanti, R.; Conrad, N.; Davis, J. J.;
608 Davison, B. H.; DeJongh, M.; Devoid, S.; Dietrich, E.; Dubchak, I.; Edirisinghe, J. N.; Fang, G.;
609 Faria, J. P.; Frybarger, P. M.; Gerlach, W.; Gerstein, M.; Greiner, A.; Gurtowski, J.; Haun, H. L.;
610 He, F.; Jain, R.; Joachimiak, M. P.; Keegan, K. P.; Kondo, S.; Kumar, V.; Land, M. L.; Meyer, F.;
611 Mills, M.; Novichkov, P. S.; Oh, T.; Olsen, G. J.; Olson, R.; Parrello, B.; Pasternak, S.; Pearson,
612 E.; Poon, S. S.; Price, G. A.; Ramakrishnan, S.; Ranjan, P.; Ronald, P. C.; Schatz, M. C.; Seaver,
613 S. M. D.; Shukla, M.; Sutormin, R. A.; Syed, M. H.; Thomason, J.; Tintle, N. L.; Wang, D.; Xia,
614 F.; Yoo, H.; Yoo, S.; Yu, D., KBase: The United States Department of Energy Systems Biology
615 Knowledgebase. *Nat. Biotechnol.* **2018,** *36*, (7), 566-569.

616 37. Thauer, R. K.; Jungermann, K.; Decker, K., Energy conservation in chemotrophic
617 anaerobic bacteria. *Bacteriol. Rev.* **1977,** *41*, (1), 100-80.

618 38. Alberty, R. A., *Thermodynamics of biochemical reactions*. John Wiley & Sons, Inc. :
619 Hoboken, New Jersey, 2003.

620 39. Andersen, S. J.; De Groof, V.; Khor, W. C.; Roume, H.; Props, R.; Coma, M.; Rabaey, K.,
621 A Clostridium Group IV Species Dominates and Suppresses a Mixed Culture Fermentation by
622 Tolerance to Medium Chain Fatty Acids Products. *Front Bioeng Biotechnol* **2017,** *5*, 8.

623 40. Roghair, M.; Hoogstad, T.; Strik, D. P. B. T. B.; Plugge, C. M.; Timmers, P. H. A.;
624 Weusthuis, R. A.; Bruins, M. E.; Buisman, C. J. N., Controlling Ethanol Use in Chain Elongation
625 by CO2 Loading Rate. *Environ. Sci. Technol.* **2018,** *52*, (3), 1496-1505.

626 41. Kucek, L. A.; Spirito, C. M.; Angenent, L. T., High n-caprylate productivities and
627 specificities from dilute ethanol and acetate: chain elongation with microbiomes to upgrade
628 products from syngas fermentation. *Energy Environ. Sci.* **2016,** *9*, (11), 3482-3494.

629 42. Weimer, P. J.; Nerdahl, M.; Brandl, D. J., Production of medium-chain volatile fatty acids
630 by mixed ruminal microorganisms is enhanced by ethanol in co-culture with Clostridium kluyveri.
631 *Bioresour. Technol.* **2015,** *175*, 97-101.

632 43. Roghair, M.; Liu, Y.; Adiatma, J. C.; Weusthuis, R. A.; Bruins, M. E.; Buisman, C. J. N.;
633 Strik, D., Effect of n-Caproate Concentration on Chain Elongation and Competing Processes. *Acs*
634 *Sustain Chem Eng* **2018,** *6*, (6), 7499-7506.

635 44. Liu, P.; Chernyshov, A.; Najdi, T.; Fu, Y.; Dickerson, J.; Sandmeyer, S.; Jarboe, L.,
636 Membrane stress caused by octanoic acid in Saccharomyces cerevisiae. *Appl. Microbiol.*
637 *Biotechnol.* **2013,** *97*, (7), 3239-51.

638 45. Weghoff, M. C.; Bertsch, J.; Muller, V., A novel mode of lactate metabolism in strictly
639 anaerobic bacteria. *Environ. Microbiol.* **2015,** *17*, (3), 670-7.

640 46. Juturu, V.; Wu, J. C., Microbial production of lactic acid: the latest development. *Crit. Rev.*
641 *Biotechnol.* **2016,** *36*, (6), 967-977.

642 47. Buschke, N.; Schafer, R.; Becker, J.; Wittmann, C., Metabolic engineering of industrial
643 platform microorganisms for biorefinery applications--optimization of substrate spectrum and
644 process robustness by rational and evolutive strategies. *Bioresour. Technol.* **2013,** *135*, 544-54.

645 48. Han, W.; He, P.; Shao, L.; Lu, F., Metabolic Interactions of a Chain Elongation
646 Microbiome. *Appl. Environ. Microbiol.* **2018**.

647 49. Scarborough, M. J.; Myers, K. S.; Donohue, T. J.; Noguera, D. R., Multi-omic analysis of
648 medium-chain fatty acid synthesis by Candidatus Weimerbacter bifidus, gen. nov., sp. nov., and
649 Candidatus Pseudoramibacter fermentans, sp. nov. In University of Wisconsin- Madison: 2019.

650 50. Zomorrodi, A. R.; Maranas, C. D., OptCom: a multi-level optimization framework for the
651 metabolic modeling and analysis of microbial communities. *PLoS Comput. Biol.* **2012,** *8*, (2),
652 e1002363.

653 51. Kumar, M.; Ji, B.; Zengler, K.; Nielsen, J., Modelling approaches for studying the
654 microbiome. *Nat Microbiol* **2019,** *4*, (8), 1253-1267.
655

FIGURES

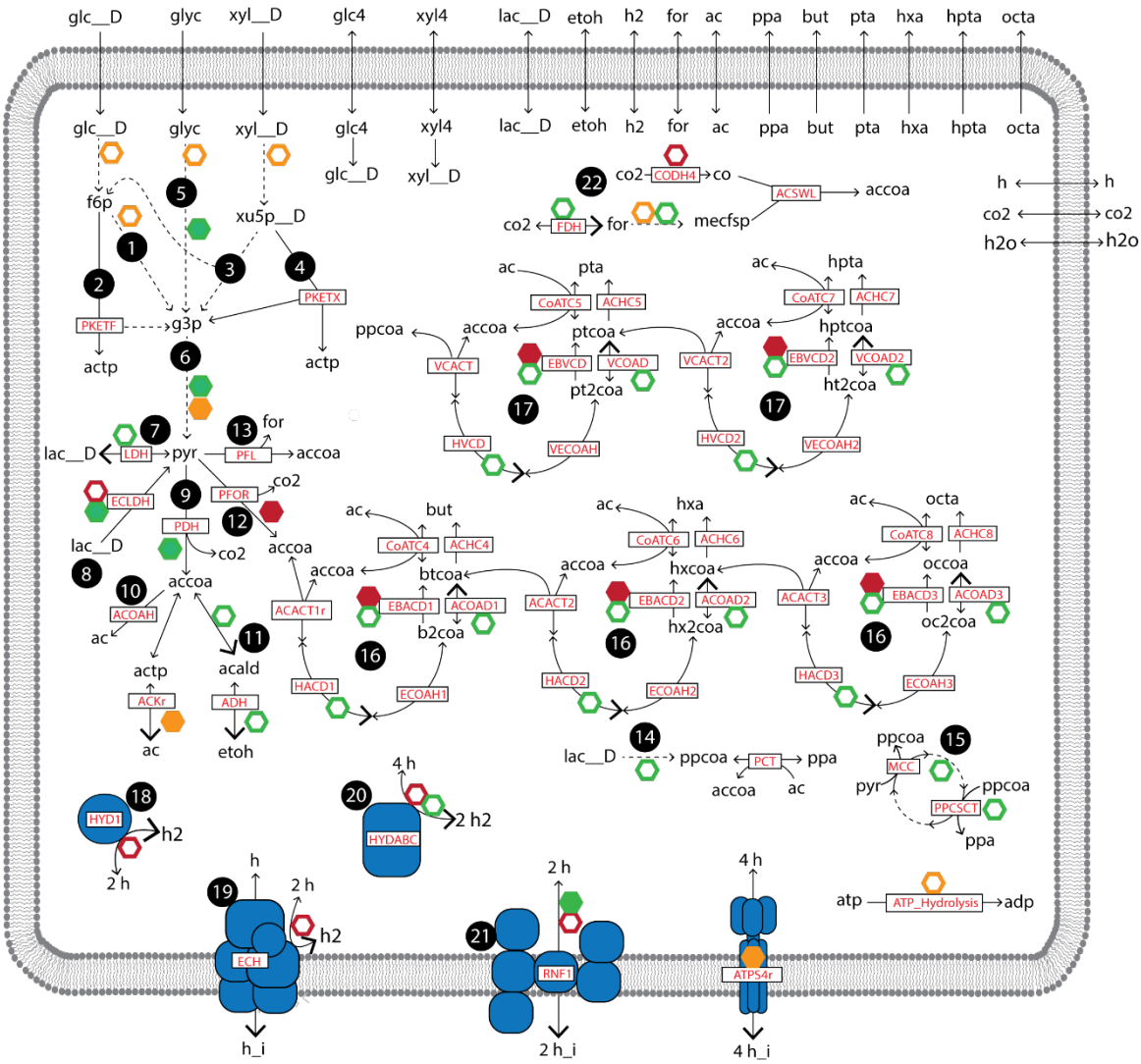

Figure 1. Summary of metabolic networks in iFerment156. Open hexagons indicate consumption of the ATP (orange), NADH (green), and reduced ferredoxin (red). Closed hexagons indicate production of these compounds and consumption of ADP (orange), NAD+ (green), and oxidized ferredoxin (red). For reversible reactions, larger arrowheads indicate the direction of the indicated compounds' consumption or production. Dashed lines indicate multiple reactions. Key reactions are indicated according to the abbreviation used in iFerment156 (**Supplementary File 3**). Pathways are identified by number: (1) upper glycolysis; (2) phosphoketolase metabolism of

665 fructose; (3) pentose phosphate; (4) phosphoketolase metabolism of xylulose; (5) glycerol
666 utilization; (6) lower glycolysis; (7) lactate metabolism via NADH-dependent lactate
667 dehydrogenase; (8) lactate metabolism via electron-confurcating lactate dehydrogenase; (9)
668 pyruvate metabolism via pyruvate dehydrogenase; (10) acetate metabolism; (11) ethanol
669 metabolism; (12) pyruvate metabolism by flavodoxin oxidoreductase; (13) pyruvate metabolism
670 by formate lyase; (14) propionate production via the acryloyl-CoA pathway; (15) propionate
671 production via the methylmalonyl-CoA pathway; (16) even-chain reverse β-oxidation; (17) odd-
672 chain reverse β-oxidation; (18) ferredoxin-dependent hydrogenase; (19) proton-translocating
673 hydrogenase; (20) electron confurcating hydrogenase; (21) the RNF complex; (22)
674 homoacetogenesis via the Wood Ljungdahl pathway. More information on the reactions and
675 metabolites contained in iFerment156 is provided in **Supplementary File 3**.

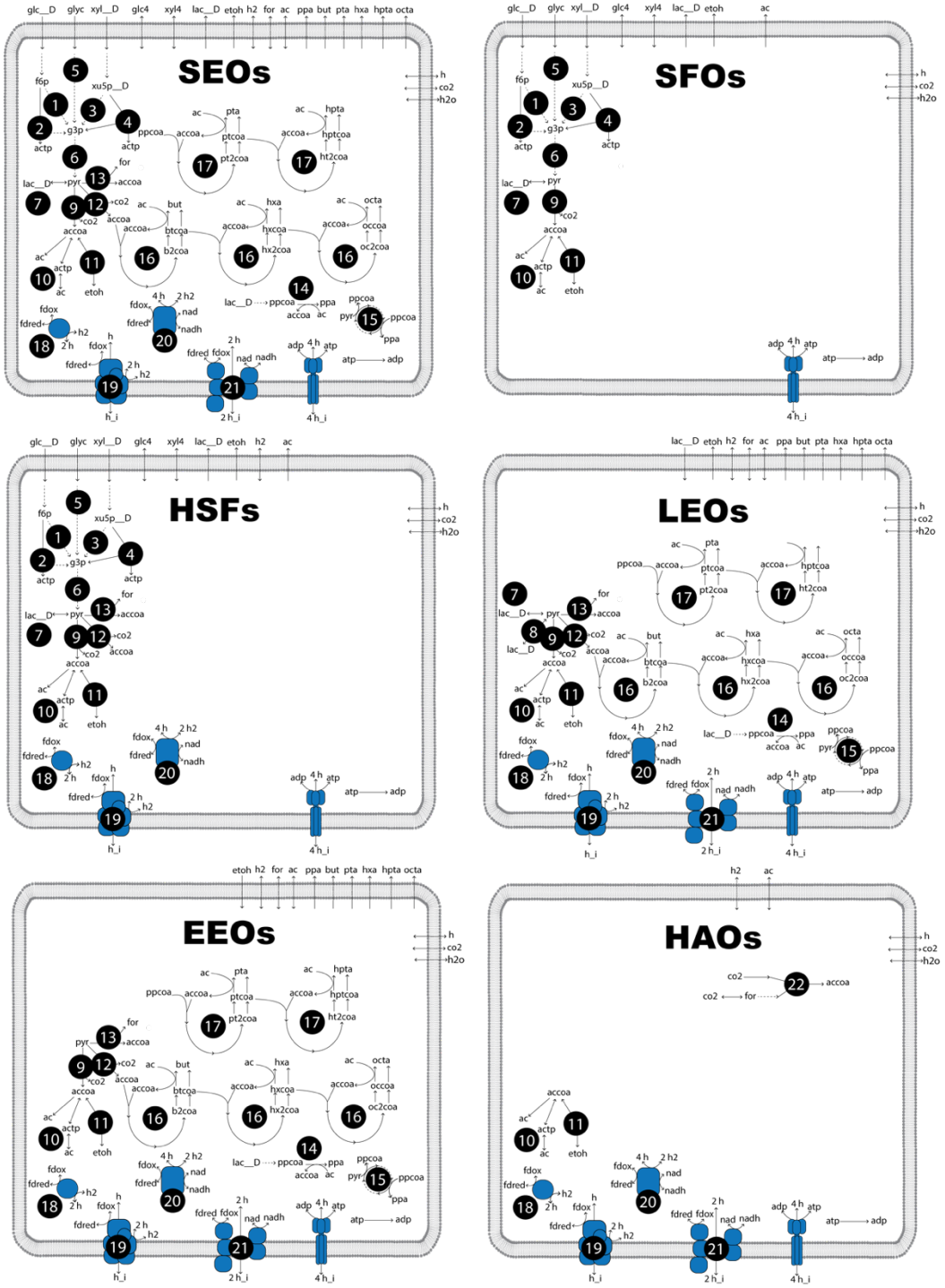

Figure 2. Summary of metabolic networks for six functional guilds contained in iFermGuilds564. Refer to Fig. 1 for details on pathways included in the iFermGuilds564 guild models. Information on the reactions and metabolites contained in the iFermGuilds564 guild models is provided in **Supplementary File 3**.

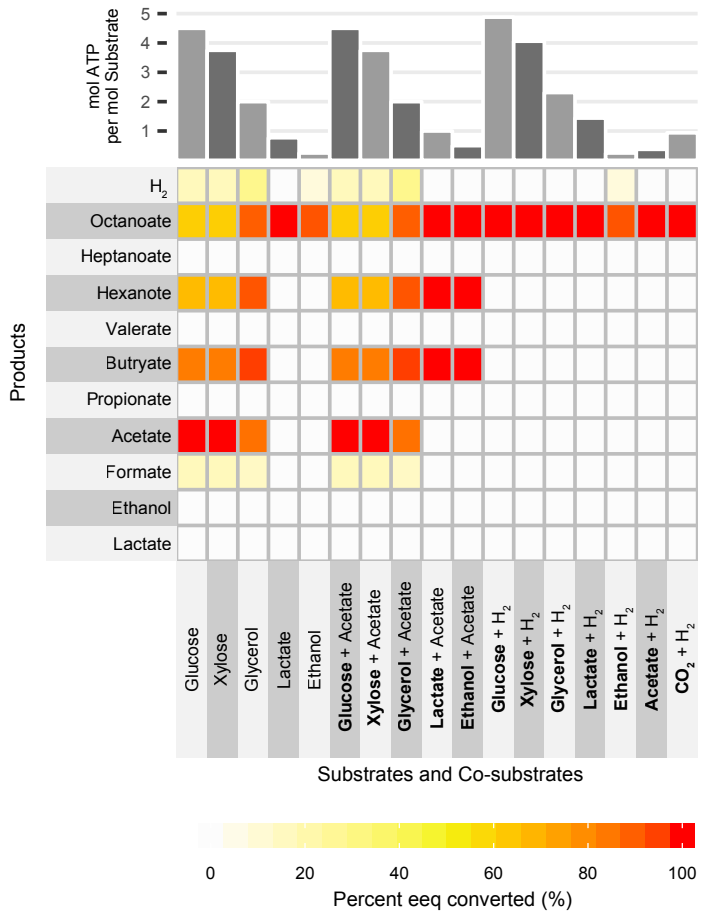

681

682 **Figure 3.** Flux variability analysis results for iFerment156 maximizing ATP production from the
683 indicated substrates. The maximum production of each end-product that can maintain the
684 maximum ATP yield is indicated. For instance, when consuming glucose, iFerment156 predicts
685 that production of formate, acetate, butyrate, hexanoate, octanoate, and H_2 can each sustain
686 maximum ATP yields. However, if lactate is the sole substrate, only octanoate production can
687 maintain the maximum ATP yield. The color intensity represents the percent of eeq that is
688 predicted by iFerment156 to be converted to the noted end-product while maintaining maximum
689 ATP production. The chart above the heatmap indicates the mol ATP generated per mol of
690 substrate utilized. For scenarios with two growth substrates, the ATP yield is relative to the
691 substrate indicated in bold text. Example model solutions are provided in Table S3.

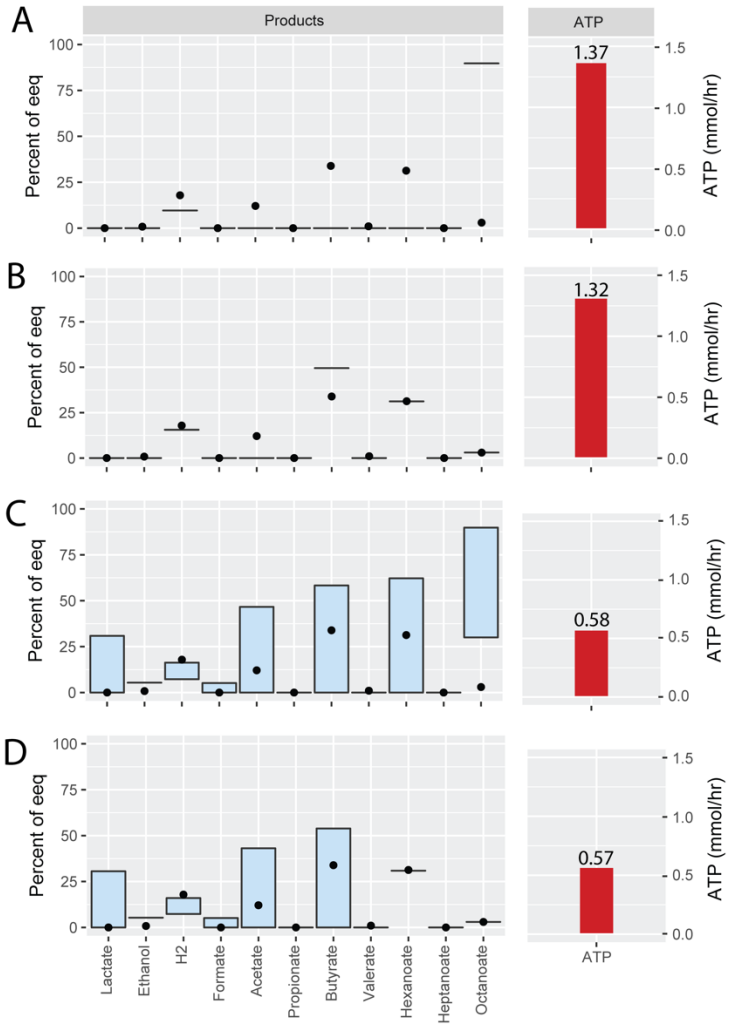

Figure 4. Predicted and observed product formation for a mixed culture fermentation bioreactor fed lignocellulosic biorefinery residues. Blue bars represent the range of products consistent with maximum ATP production by the microbial community. Products represented by black lines indicate there is a unique percent of eeq that must be converted to that compound. Closed black circles represent the observed level of product accumulated in a bioreactor fed lignocellulosic biorefinery residues (A) predictions with iFerment156; (B) predictions with iFerment156 with constrained hexanoate and octanoate production; (C) predictions with iFermGuilds564; (D) predictions with iFermGuilds564 with constrained hexanoate and octanoate production.

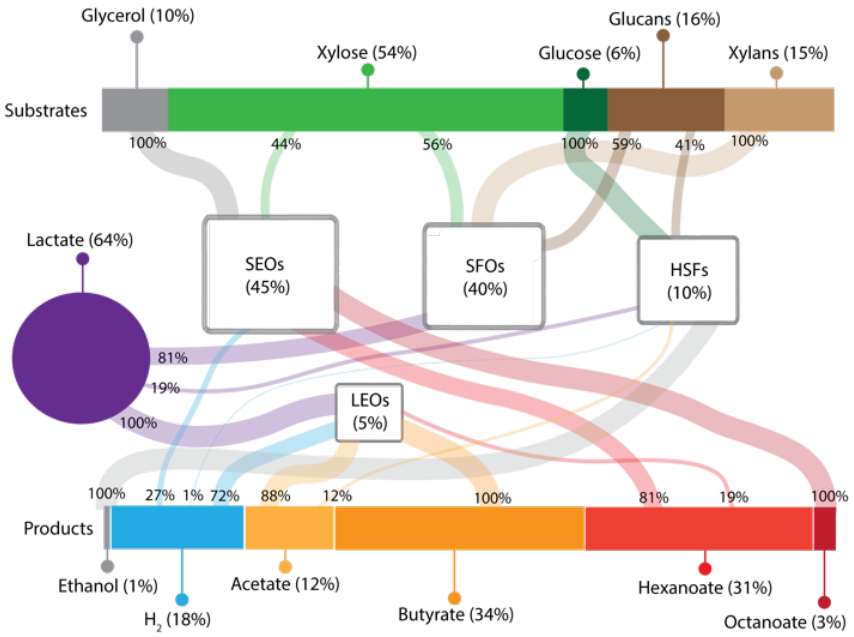

Figure 5. Predicted substrate flow through a mixed culture fermentation producing a mixture of MCFA from a complex feedstock using iFermGuilds564. Values were obtained using pFBA while constraining the products according to observed bioreactor performance. The relative abundance of each functional guild assumed based on reactor DNA sbundance is given in parentheses. The relative amount of eeq in the substrates, products, and intermediates are also provided. Line width indicates the relative amount of each substrate consumed and product produced by each of the functional guilds. H_2 was not measured, so for these simulations it was assumed that the difference between eeq in the substrate and eeq in the measured soluble and insoluble products represented H_2 production. In this simulation, 64% of the eeq in conversion residue was predicted to be directed to lactate as an intermediate.

714

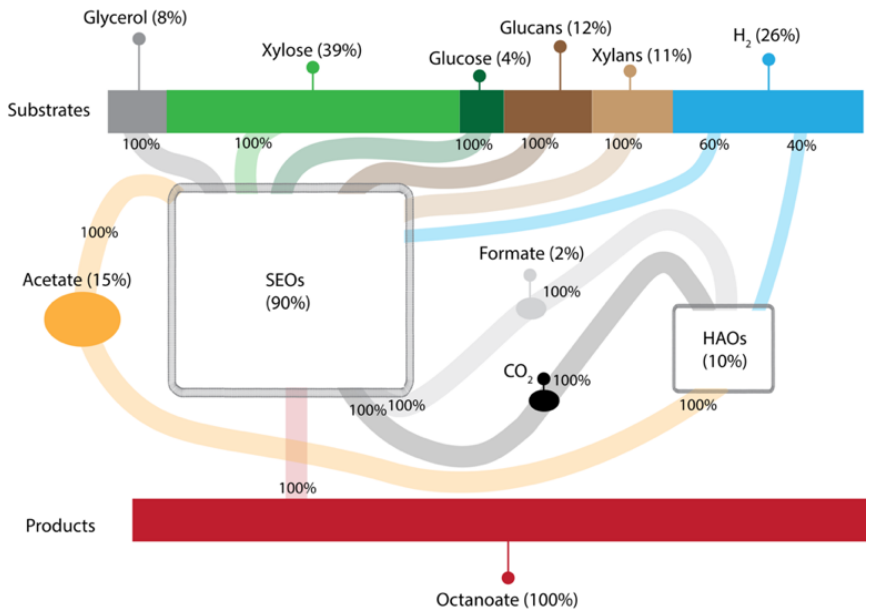

715

716 **Figure 6.** iFermGuilds564 predicted fluxes through a community of SEOs and HAOs converting

717 lignocellulosic biorefinery residue and exogenous H_2 into octanoate. SEOs provide CO_2 and

718 formate to the HAOs, while the HAOs provide acetate to SEOs.